Multitribe evolutionary search for stable Cu-Pd-Ag nanoparticles using neural network models

Samad Hajinazar, Ernesto D. Sandoval, Aiden J. Cullo, and Aleksey N. Kolmogorov
Department of Physics, Applied Physics and Astronomy,
Binghamton University, State University of New York,
PO Box 6000, Binghamton, New York 13902-6000, USA
(Dated: March 14, 2019)

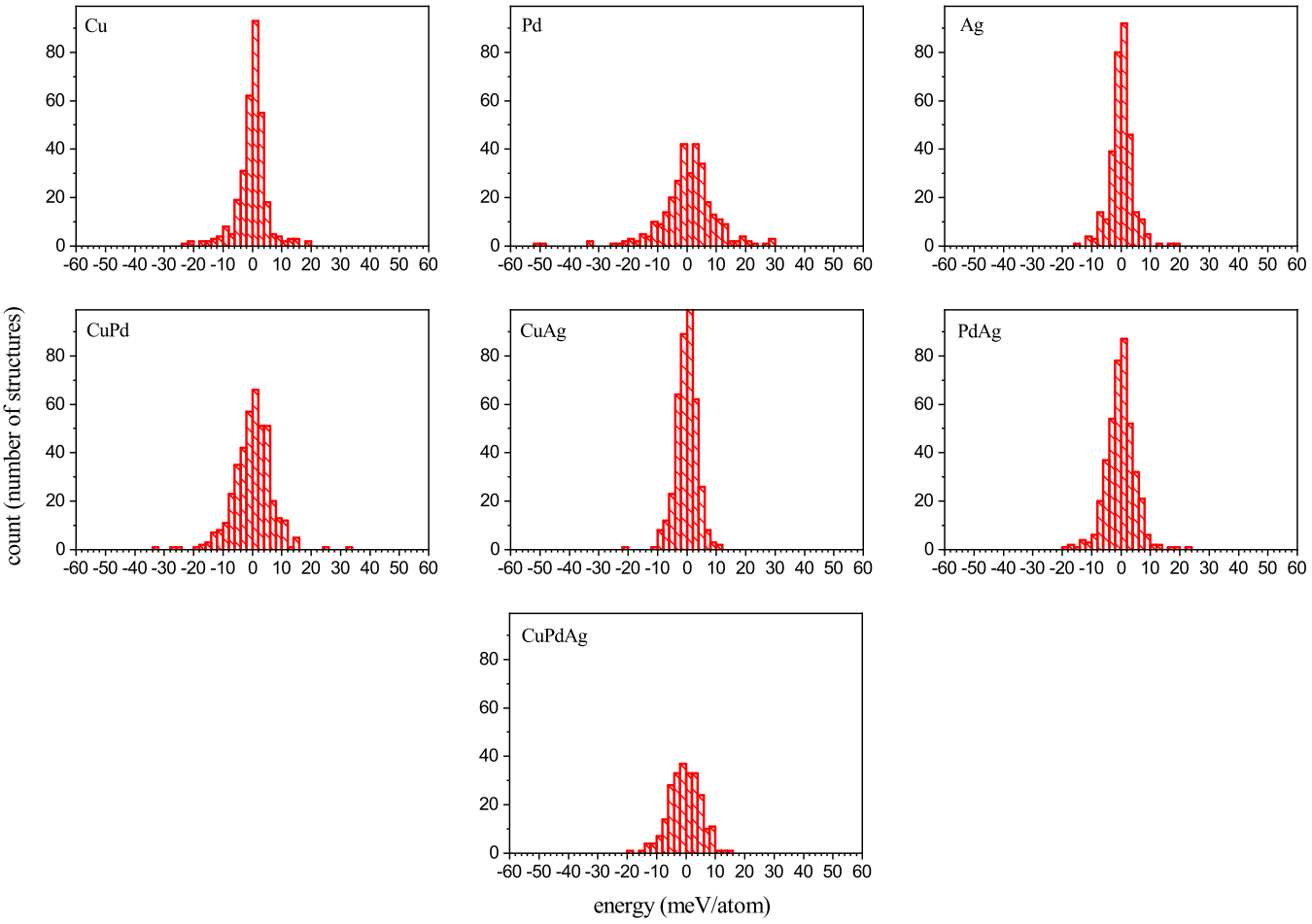

FIG. S1: Distribution of total energy errors (meV/atom) for the testing sets of the NN model for each compound, with respect to the GGA reference energies.

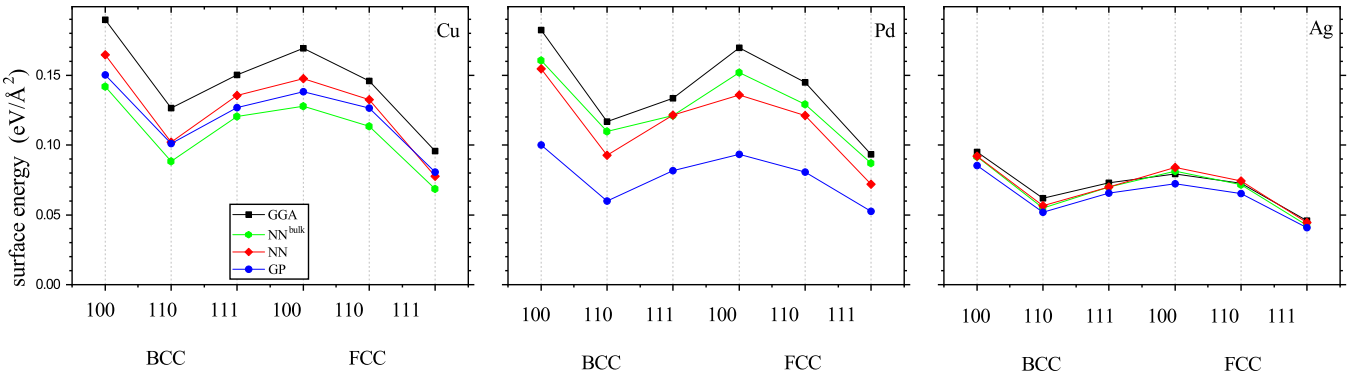

FIG. S2: Surface energies of elemental high-symmetry structures (BCC and FCC) for selected surfaces (100, 110, and 111) evaluated with NN^{bulk}, NN, GP, and the GGA. In all these tests, we used the GGA-optimized structures: the slabs had relaxed atomic positions with the in-plane lattice constants fixed at the corresponding bulk values of 2.876, 3.163, and 3.311 Å for

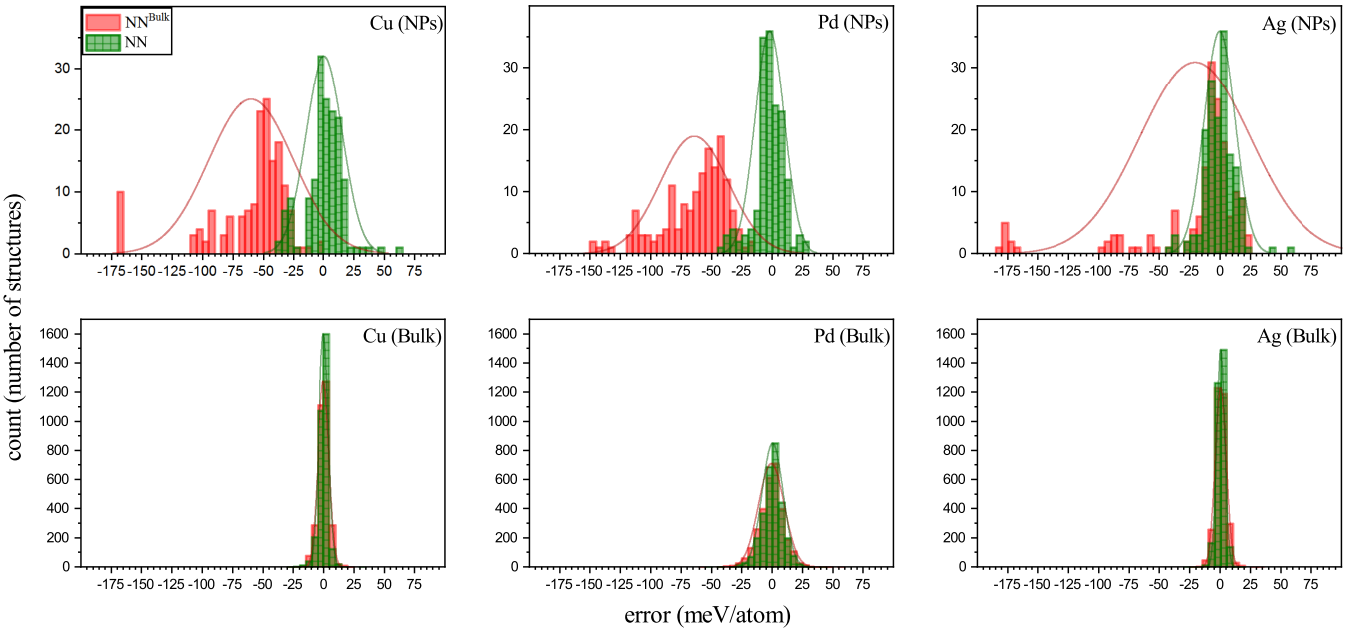

FIG. S3: Distribution of testing errors (meV/atom) for elemental bulk and NP datasets evaluated with NN$^{\text{bulk}}$ and NN models, with respect to GGA reference energies.

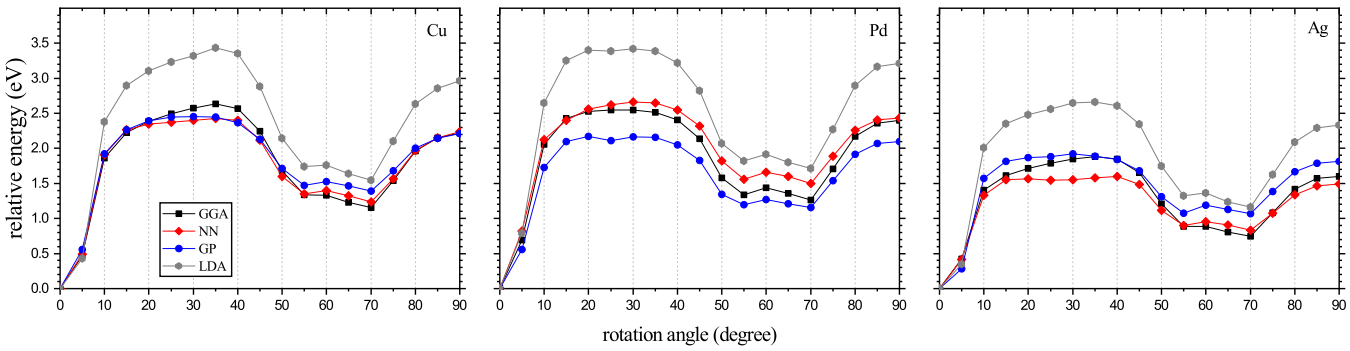

FIG. S4: Relative energy profiles evaluated with different methods for elemental 55-atom NPs, in which one atom is moved along the surface. The starting reference configuration is an ideal icosahedron structure fully relaxed with the GGA. At each step, the selected atom is rotated by 5° and its radial distance is optimized with the GGA while the rest of the NP is kept fixed.

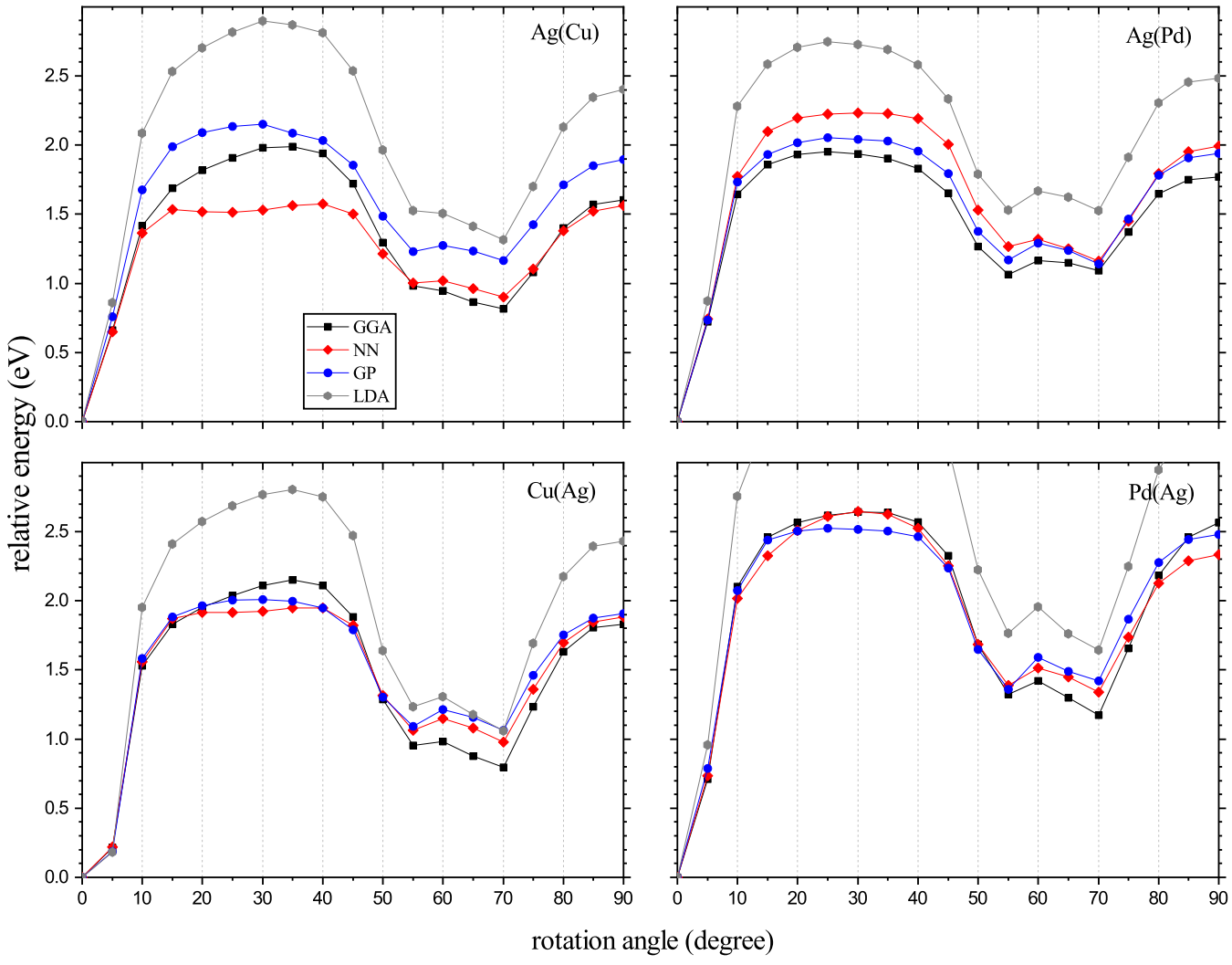

FIG. S5: Same as in Fig. S4 for binary A(B) NPs, in which one metal atom A is rotated about the NP comprised of metal B.

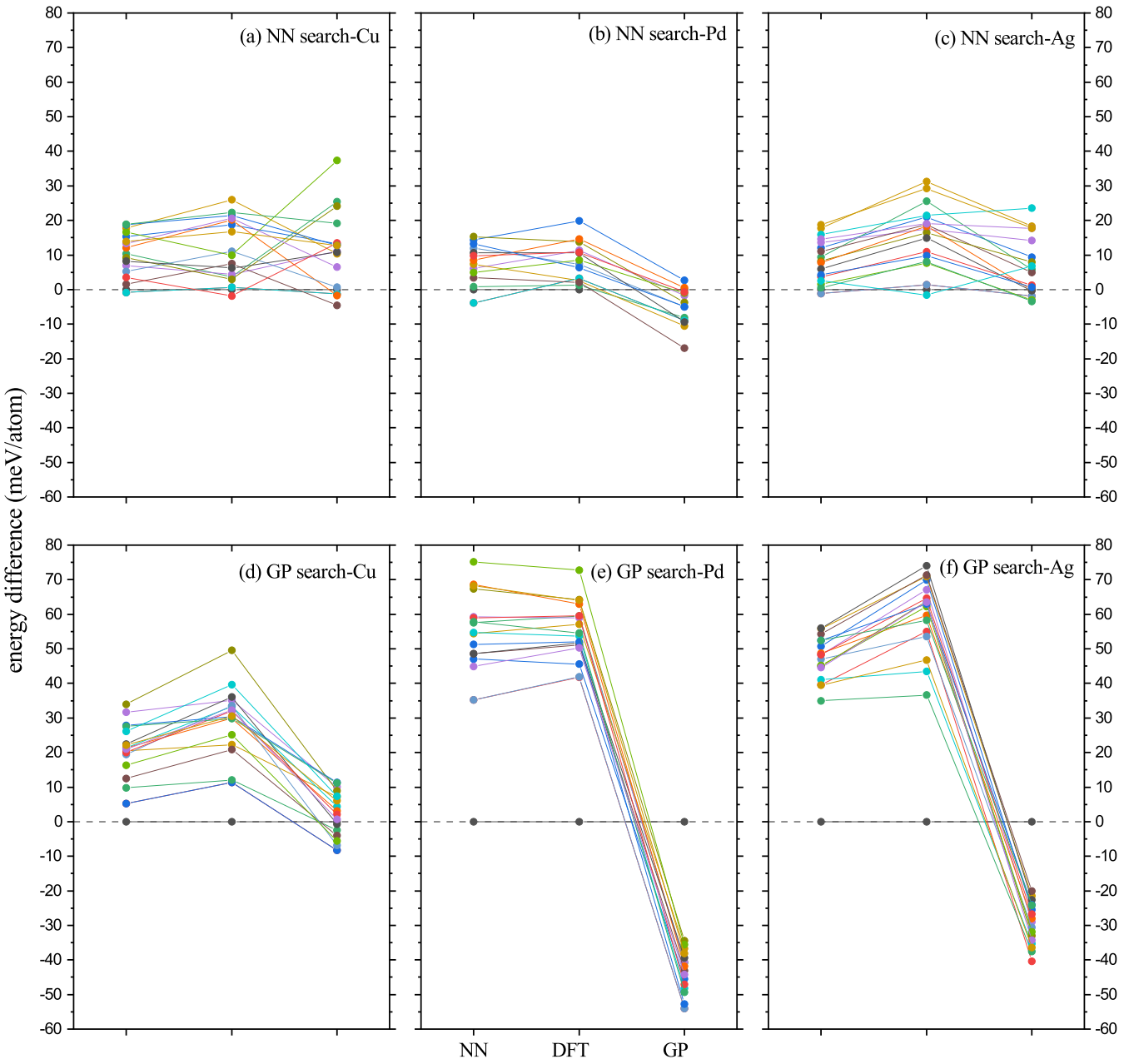

FIG. S6: GGA relative energy of low-energy structures found with NN-based searches (panels (a,b,c)) and GP-based searches (panels (d,e,f)). Each pools consists of select structures within 20 meV/atom of the putative ground state. In each panel, the structures shown on the left, in the middle, and on the right were fully relaxed with the NN, GGA, and GP, respectively, and their energies were evaluated with single-point GGA calculations. The plot illustrates that the GGA energies of GP-relaxed structures exhibit poor correlation with the GGA energies after the ab initio relaxation.

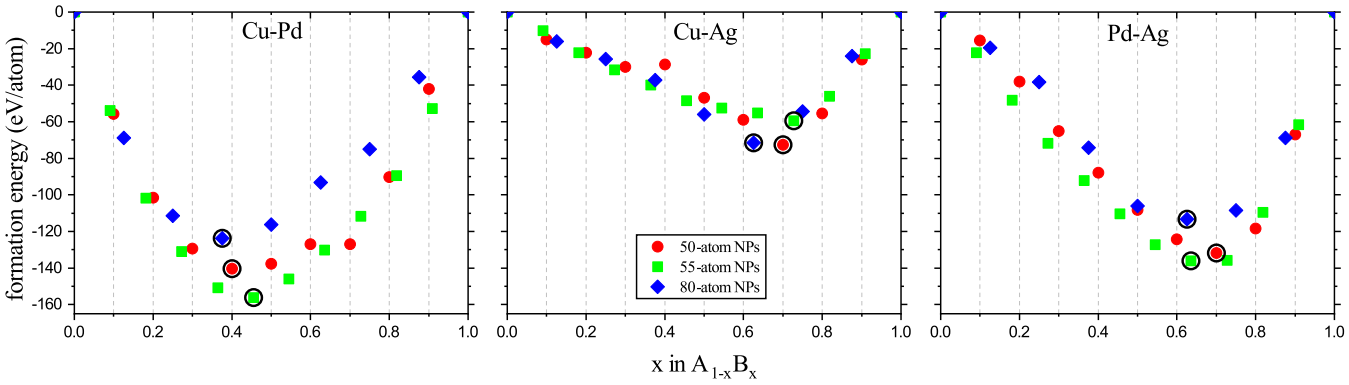

FIG. S7: Formation energy of putative ground states for bimetallic NPs of various sizes, evaluated by the NN model. The lowest energy composition ratio for each size is highlighted with a circle.

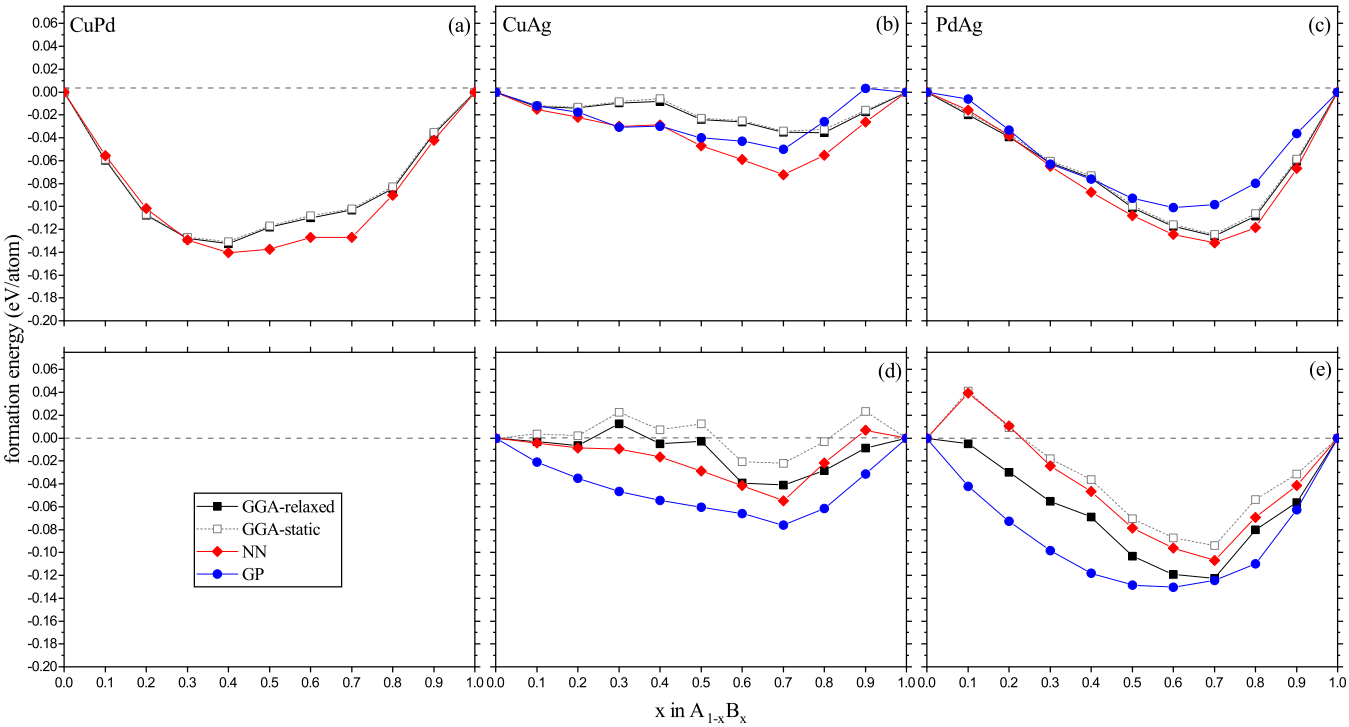

FIG. S8: Formation energy of binary NPs found with NN- (upper panels) and GP-based (lower panels) searches. The diamond (red) and circle (blue) points are demonstrating the formation energy evaluated with NN and GP, respectively. The empty and solid (black) squares are GGA formation energies of structures and of their GGA-optimized form, respectively.

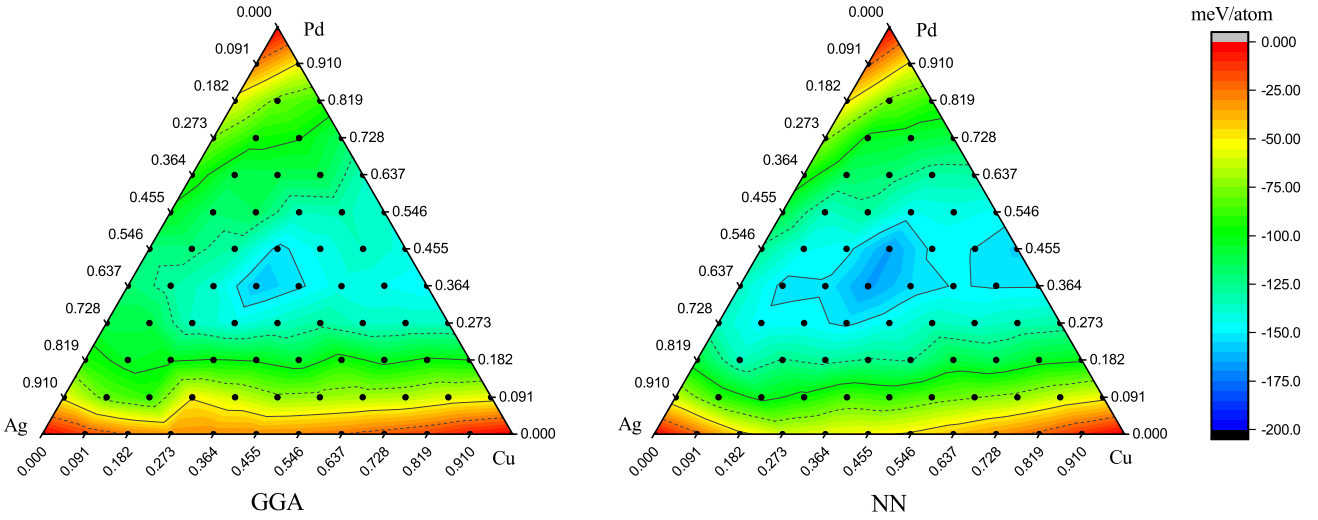

FIG. S9: Color-coded relative formation energies of the 55-atom NPs of the Cu-Pd-Ag ternary system, calculated with the GGA and NN.

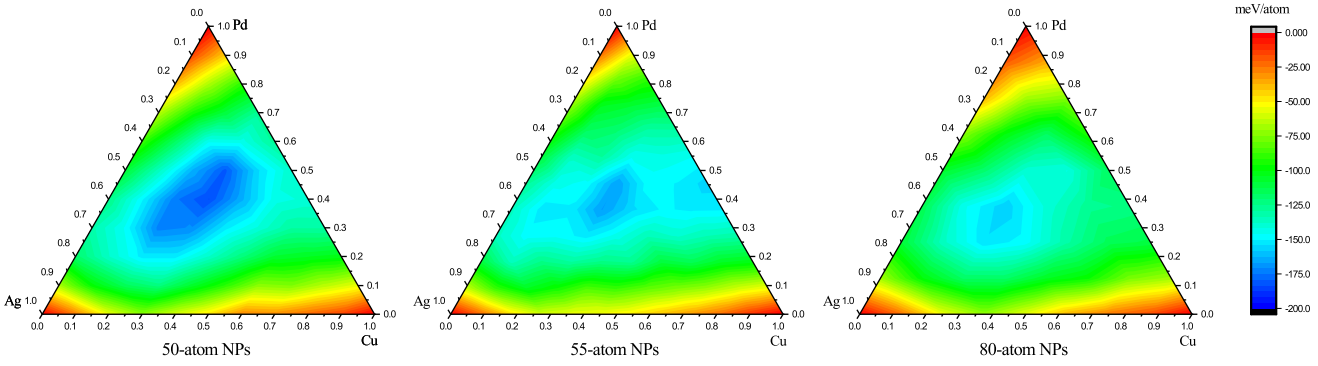

FIG. S10: Color-coded relative formation energies of 50-, 55-, and 80-atom NPs for Cu-Pd-Ag ternary system, calculated with NN model.

element	size	PBE	RPBE	LDA
Cu	31	−6.81	−8.09	−4.21
	36	−14.94	−13.17	−17.81
	37	5.74	3.68	10.2
	43	−7.03	−7.82	−5.42
	44	−13.92	−13.88	−14.24
	48	−20.82	−22.24	−17.82
	51	−23.58	−23.92	−23.26
	52	−9.54	−9.96	−9.25
	66	−4.12	−4.1	−3.89
	80	−3.86	−2.66	−6.33
Pd	31	−6.98	−7.81	−3.19
	32	−7.06	−9.14	−2.63
	41	−23.21	−20.36	−29.44
	43	−15.29	−12.63	−21.65
	44	−21.54	−18.8	−28.24
	53	−11.69	−11.12	−15.62
	60	−14.23	−13.89	−15.59
	65	−8.39	−7.92	−10.81
	66	−6.97	−7.28	−8.22
	80	−0.02	0	−0.01
Ag	30	−3.45	−5.23	−0.46
	31	−7.24	−7.63	−7.06
	32	−5.92	−7.66	−3.63
	33	−1.56	−1.07	−2.5
	34	1.92	1.16	2.9
	35	−7.51	−6.79	−9.13
	36	−14.96	−17.21	−11.23
	37	−10.06	−8.71	−11.2
	40	−6.74	−8.93	−3.1
	41	2.41	1.74	4.05

TABLE S1: Energy difference (in meV/atom units) for the NPs found with the NN-based search over the GP-based structures for a subset of the elemental NPs. The energy changes are obtained by optimizing both the NN- and GP-based results with various exchange-correlation functionals within DFT approach.

system	average	std. dev.	maximum
Cu	0.92	0.02	40.67
Pd	1.13	0.03	49.09
Ag	0.98	0.02	31.61
CuPd	1.14	0.02	55.43
CuAg	0.92	0.01	43.93
PdAg	1.01	0.01	45.03
CuPdAg	0.74	0.01	10.63

TABLE S2: Average, standard deviation, and maximum of the atomic force magnitudes (in eV/Å) in the training dataset for NN models. The large value of the maximum force in elemental and binary datasets is due to presence of a few high-energy clusters that are sampled to ensure the correct behavior of the interaction model in short interatomic distance regimes.

No.	Type	Rc	Rs	η	ζ	λ
1	pair	7.5	0.0000	0.000 64	1.0000	−1.0000
2	pair	7.5	0.0000	0.0064	1.0000	−1.0000
3	pair	7.5	0.0000	0.0128	1.0000	−1.0000
4	pair	7.5	0.0000	0.0224	1.0000	−1.0000
5	pair	7.5	0.0000	0.0384	1.0000	−1.0000
6	pair	7.5	0.0000	0.064	1.0000	−1.0000
7	pair	7.5	0.0000	0.128	1.0000	−1.0000
8	pair	7.5	0.0000	0.256	1.0000	−1.0000
9	triplet	7.5	0.0000	0.000 64	1.0000	−1.0000
10	triplet	7.5	0.0000	0.000 64	1.0000	1.0000
11	triplet	7.5	0.0000	0.000 64	2.0000	−1.0000
12	triplet	7.5	0.0000	0.000 64	2.0000	1.0000
13	triplet	7.5	0.0000	0.001 92	1.0000	−1.0000
14	triplet	7.5	0.0000	0.001 92	1.0000	1.0000
15	triplet	7.5	0.0000	0.001 92	2.0000	−1.0000
16	triplet	7.5	0.0000	0.001 92	2.0000	1.0000
17	triplet	7.5	0.0000	0.005 12	1.0000	−1.0000
18	triplet	7.5	0.0000	0.005 12	1.0000	1.0000
19	triplet	7.5	0.0000	0.005 12	2.0000	−1.0000
20	triplet	7.5	0.0000	0.005 12	2.0000	1.0000
21	triplet	7.5	0.0000	0.0096	1.0000	−1.0000
22	triplet	7.5	0.0000	0.0096	1.0000	1.0000
23	triplet	7.5	0.0000	0.0096	2.0000	−1.0000
24	triplet	7.5	0.0000	0.0096	2.0000	1.0000
25	triplet	7.5	0.0000	0.0096	4.0000	−1.0000
26	triplet	7.5	0.0000	0.0096	4.0000	1.0000
27	triplet	7.5	0.0000	0.0096	16.0000	−1.0000
28	triplet	7.5	0.0000	0.0096	16.0000	1.0000
29	triplet	7.5	0.0000	0.016	1.0000	−1.0000
30	triplet	7.5	0.0000	0.016	1.0000	1.0000
31	triplet	7.5	0.0000	0.016	2.0000	−1.0000
32	triplet	7.5	0.0000	0.016	2.0000	1.0000
33	triplet	7.5	0.0000	0.016	4.0000	−1.0000
34	triplet	7.5	0.0000	0.016	4.0000	1.0000
35	triplet	7.5	0.0000	0.016	16.0000	−1.0000
36	triplet	7.5	0.0000	0.016	16.0000	1.0000
37	triplet	7.5	0.0000	0.0288	1.0000	−1.0000
38	triplet	7.5	0.0000	0.0288	1.0000	1.0000
39	triplet	7.5	0.0000	0.0288	2.0000	−1.0000
40	triplet	7.5	0.0000	0.0288	2.0000	1.0000
41	triplet	7.5	0.0000	0.0288	4.0000	−1.0000
42	triplet	7.5	0.0000	0.0288	4.0000	1.0000
43	triplet	7.5	0.0000	0.0288	16.0000	−1.0000
44	triplet	7.5	0.0000	0.0288	16.0000	1.0000
45	triplet	7.5	0.0000	0.0512	1.0000	−1.0000
46	triplet	7.5	0.0000	0.0512	1.0000	1.0000
47	triplet	7.5	0.0000	0.0512	2.0000	−1.0000
48	triplet	7.5	0.0000	0.0512	2.0000	1.0000
49	triplet	7.5	0.0000	0.0512	4.0000	−1.0000
50	triplet	7.5	0.0000	0.0512	4.0000	1.0000
51	triplet	7.5	0.0000	0.0512	16.0000	−1.0000

TABLE S3: Behler-Parrinello symmetry functions: the set of functions and coefficients used in this paper as 51 components of the input vector. The η parameter's values are rescaled compared to the original set of coefficients that are introduced by Behler-Parrinello to account for the change in cutoff radius from 6 to 7.5 Å.